A performance analysis model with thermodynamic and superficial effects of the touchdown bearings in AMB systems

Mindong LV*, Zixi WANG* and Yuming WANG*

*Department of Mechanical Engineering, Tsinghua University

Haidian District, Beijing, 100084, China

E-mail: lmd13@mails.tsinghua.edu.cn

Abstract

The touchdown bearing is one of the essential parts of AMB. When the magnetic bearing fails, touchdown events will occur and the rub-impact between the rotor and the touchdown bearings will happen. In practice, the analysis of the process is complex as it is coupled with dynamics, superficial and thermal effects. A simulation model in which the kinetic equations of the rotor and the bearing are derived from Lagrange's equations and the drag torque of the ball bearings is calculated by Palmgren's empirical formula has been established. The simulation results show that the orbit response of the pendulum vibration appears when the rotating speeds and the friction coefficients are low, while the orbit response of the backward whirl appears when the rotating speeds and the friction coefficients are high. The critical whirl speed has been illustrated for the guidance of the safe landing of the rotor. The maximum contact forces and heat peak power have also been calculated. The maximum contact forces keep almost constant when both the rotating speeds and the friction coefficients are low. It increases with the growth of the rotating speed and the friction coefficient with high rotating speeds, high friction coefficients or both. The peak thermal power increases with the incline of the rotating speeds and friction coefficients.

Keywords : Friction coefficient, Backward whirl, Simulation, Touchdown bearing, AMB

1. Introduction

Active Magnetic Bearings (AMB) have been increasingly used in the rotary machines. Compared with the traditional bearings, AMBs have many advantages such as non-friction, low loss, low noise and adjustable stiffness and damping.

The touchdown bearing is one of the key elements in the AMB systems. It provides backup protection of the system. When the rotor fails to be suspended by AMBs, touchdown bearings will support it and prevent the damage caused by the severe rub-impact of the rotor and the stator.

At present, rolling element bearings are generally used as touchdown bearings in AMBs. When the horizontal rotor drops onto the touchdown bearings, it may exhibit a number of orbit responses including: pendulum vibration, combined rub and bouncing, and the backward whirl. Bounces happen at the first several times of contacts between the rotor and the inner race. In this stage, the inner race of the bearing is accelerated the contact forces and the friction are relatively high. Afterwards, the rotor will enter the state of motion of either pendulum vibration or backward whirl. Pendulum vibration is a steady state of motion and the vibration frequency of the rotor is almost fixed due to the low friction acts on it. Backward whirl is the most violent motion with high whirl frequency, heavy contact forces and friction.

Early studies of the touchdown events in AMB can be found in the dissertation of M.Fumagalli (1993). Theoretical and experimental studies were carried out using various kinds of touchdown bearings, such as bronze rings, graphite rings and rolling element bearings. The rotor orbits and contact forces were both simulated and measured. The transient behavior of the rotor during the touchdown events was analyzed by Zeng (2002, 2003) theoretically and experimentally. The dynamic behavior of the touchdown events with the touchdown bearings misaligned mounted was researched by Kärkkäinen et al. (2006, 2007) numerically. The simulated obits and the contact forces were verified by the experiments. Thermal effects when the rotor drops onto the touchdown bearings were numerically studied by G.Sun (2003). Power loss and heat generation were calculated in the model. Lee et al. (2012) theoretically predicted the life of the touchdown

bearing using a rainflow counting method. Zhao (2016) numerically analyzed the thermal growth based on the Hertzian contact model and a 1D thermal heat transfer network model.

In this paper, the dynamic and thermal model of the touchdown events have been established. The orbit responses, critical whirl speeds, the maximum contact forces and the peak thermal power have been analyzed. Finally, conclusions have been made.

2. Dynamic model of the rotor system

The dynamic model of the rotor-bearing system during the touchdown events is established in this section. Figure 1 shows the simplified model of the rotor and the touchdown bearing. Hertzian contact model is used for the calculation of contact forces between the rotor and the inner race. The stiffness and the friction torque of the touchdown bearings has been derived by Harris (2007).

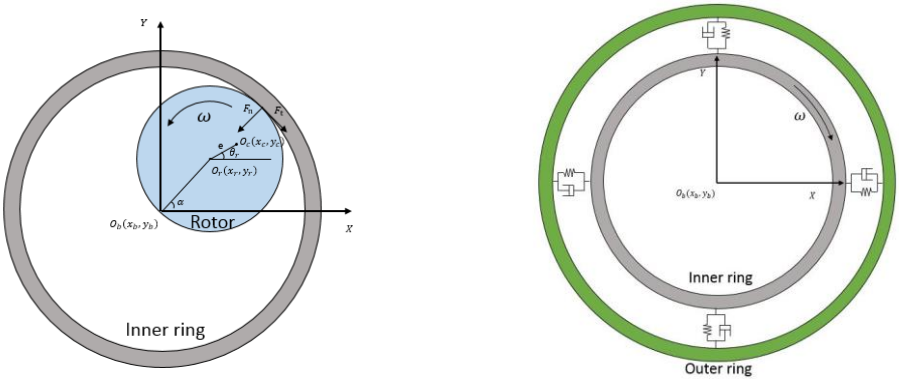

(a) (b)

Fig. 1 The dynamic model of the rotor-bearing system. The contact forces and friction forces between the rotor and inner race are illustrated in Fig.1 (a), including the rotor (blue) and the inner ring of the touchdown bearing (gray). The contact forces and friction forces inside the touchdown bearing are as Fig.1 (b), including the inner ring (gray) and the outer ring (green). O_b indicates the geometric center of the inner race, O_r is the geometric center of the rotor and O_c is the center of mass of the rotor.

2.1 Kinetic model of the rotor-bearing system

The dynamic characteristics of the touchdown events can be derived from the kinetic equations of the rotor-bearing system. The equations are derived from Lagrange`s equations.

$$m_r\left(\ddot{x}_r - e\ddot{\theta}_r sin\theta_r - e\dot{\theta}_r^2\, cos\theta_r\right) = -F_{n1}cos\alpha + F_{t1}sin\alpha \tag{1}$$

$$m_r(\ddot{y}_r + e\ddot{\theta}_r cos\theta_r - e\dot{\theta}_r^2\, sin\theta_r + g) = -F_{n1}sin\alpha - F_{t1}cos\alpha \tag{2}$$

$$J_r\ddot{\theta}_r = -F_{t1}r - m_r gecos\theta_r \tag{3}$$

where F_{n1} is the radial contact force of the rotor and the inner race of the bearing, F_{t1} is the friction force of the rotor and the inner race, α is the contact angle of rotor and the inner race (shown in Fig.1 (b)).

The kinetic equations of the inner race of the bearing are as follows:

$$m_{\mathrm{b}}\ddot{x}_b = F_{n1}cos\alpha' + F_{t1}sin\alpha' - F_{n2}cos\beta - F_{t2}sin\beta \tag{4}$$

$$m_{\mathrm{b}}\ddot{y}_b = m_b g + F_{n1}sin\alpha' - F_{t1}cos\alpha' - F_{n2}sin\beta - F_{t2}cos\beta \tag{5}$$

$$J_{\mathrm{b}}\ddot{\theta}_b = (F_{t2} - F_{t1})(s + r) \tag{6}$$

where F_{n2} is the contact force between the inner race and rolling elements, F_{t2} is the friction force between the inner race and rolling elements, β is the contact angle between the inner race and the rolling elements.

2.2 Model of contact

The contact model in this section includes the descriptions of the radial contact force and friction.

During the drop process, the rotor and the bearing will contact in the radial direction. Based on the Hertzian contact model, the contact force is described as follows:

$$F_n = \begin{cases} K\delta^e + C\dot{\delta}, & \delta > 0 \\ 0, & \delta < 0 \end{cases} \tag{7}$$

where δ is the impact depth, K is the contact stiffness, C is the contact damping, e is the contact coefficient (e=10/9 for line contact, e=3/2 for point contact).

Friction is described as follows:

$$F_t = \text{sign}(V_r - V_i) \cdot \mu_d F_n \tag{8}$$

where μ_d is the dynamic friction coefficient between the rotor and the inner race, V_r and V_i are velocity of the rotor and the inner race respectively at the contact point.

When the tangential velocity of the inner race equals the rotor, the rolling condition is satisfied:

$$\dot{\theta}_b R_b = \dot{\theta}_r R_r + \dot{\theta}_w s \tag{9}$$

where $\dot{\theta}_b$, $\dot{\theta}_r$ are the rotating velocity of the inner race and rotor, respectively; $\dot{\theta}_w$ is the translational velocity of the center of the rotor.

Rolling friction can be calculated by equations (1-6) and (9). The judgment of slipping or rolling contacts is:

$$\begin{cases} F_t > \mu_s F_n, & \text{slipping again} \\ F_t \le \mu_s F_n, & \text{keep rolling} \end{cases} \tag{10}$$

where μ_s is the maximum static friction coefficient.

2.3 Friction drag torque and heat generation

The friction drag torque M inside the bearing is calculated by Palmgren`s empirical formula (2007),

$$M = M_0 + M_1 \tag{11}$$

$$M_0 = \begin{cases} 10^{-7} f_0 (v_0 n)^{\frac{2}{3}} d_m^3, & v_0 n > 2000 \\ 160 * 10^{-7} f_0 d_m^3, & v_0 n \le 2000 \end{cases} \tag{12}$$

$$M_1 = f_1 P_1 d_m \tag{13}$$

where M_0 is the friction torque due to viscosity of bearing lubricant and inner race speed, M_1 is the friction torque due to external loads in the bearing. f_0 is the factor depends on the bearing type and lubrication, v_0 is the kinematic viscosity of the lubricant. n is the angular velocity of the inner race. f_1 is the factor depending on the bearing design and relative bearing load, P_1 is the equivalent dynamic load.

The total heat generation H is as follows.

$$H = H_i + H_o + H_s \tag{14}$$

$$H_i = \omega_r * \sum_j M_{ij} + \omega_{si} * M_{si} \tag{15}$$

$$H_o = \omega_r * \sum_j M_{oj} + \omega_{so} * M_{so} \tag{16}$$

$$H_s = F_t \cdot v_{rel} \tag{17}$$

where H_i, H_o, H_s are the heat generation at the contacts between the balls and the inner race, the balls and the outer race, and between the rotor and the inner race respectively. ω_r, ω_{si}, ω_{so} are the angular velocity of the rotor, and the ball spinning angular velocity at the inner and outer race contact surface, respectively. M_{ij}, M_{oj} are the friction torque of the jth ball at the inner race and outer race, respectively. M_{si}, M_{so} are the spinning moments at the inner and outer race. v_{rel} is the relative speed between the rotor and the inner race.

3. Thermal model of the rotor system

3.1 Heat transfer network

Heat transfer in the touchdown bearing is actually 3 dimensional. Assuming that the heat flux is distributed equally in the radial direction and symmetrically in the axial direction, one-dimensional thermal model is established. Each part is described as a bulk heat mass. The heat transfer in the equations is described by thermal resistances as the connectors between interested temperature nodes.

The thermal resistance of the key components of the rotor-bearing system are shown in Table 1. λ_i, λ_e are the heat conductivity coefficient of the inner race and outer race, respectively, W is the width of the component, L is the length of the component,

The heat transfer process between each temperature node can be described by the following first order thermal equation.

$$mC\Delta T = \Delta Q \tag{18}$$

where m indicates the mass of each part, C indicates the specific heat, Q indicates the heat flux of each part.

The thermal equations for each temperature node are:

$$m_s C_{ps} \frac{dT_s}{dt} = \frac{H_r}{2} - \frac{T_s - T_i}{R_{sr}} - \frac{T_s - T_\infty}{R_{sac} + R_{sav}} \tag{19}$$

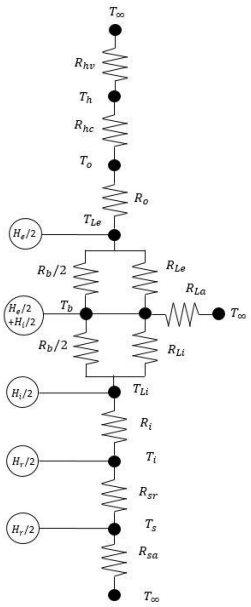

Fig. 2 Heat transfer network of the touchdown bearing. T indicates the temperature at each nodes. R is the thermal resistance of each part. H is the heat generation. The subscript i, o indicates the inner and outer ring respectively, b represents the ball, L represents the lubricant, h represents the housing.

Table 1 Thermal resistances of heat transfer network

	Thermal resistances
Inner race / Outer race	$R_i = \frac{\ln(r_i/r_s)}{2\pi\lambda_i W}$, $R_e = \frac{\ln(r_o/r_e)}{2\pi\lambda_e W}$
Rotor	$R_{sac} = \frac{L_s}{\lambda_s \pi r_s^2}$, , $R_{sav} = \frac{1}{h_s \pi r_s^2}$, $R_{sr} = \frac{1}{\lambda_s \pi W_i}$, $R_{sa} = \frac{R_{sac} \cdot R_{sav}}{R_{sac}+R_{sav}}$
Housing	$R_{hac} = \frac{L_h}{2\pi\lambda_h(r_h^2-r_o^2)}$, $R_{hav} = \frac{1}{\pi h_h(r_h^2-r_o^2)}$, $R_{ha} = R_{hac} + R_{hav}$ $R_{hrc} = \frac{\ln(r_h/r_o)}{2\pi\lambda_h L_h}$, $R_{hrv} = \frac{1}{2\pi r_h L_h h_h}$, $R_{hr} = R_{hrc} + R_{hrv}$
Ball / lubricant	$R_b = \frac{1}{z\lambda_b \pi r_b}$, $R_{Li} \approx \frac{r_b}{\lambda_l(2\pi r_i W_i - n\pi r_b^2)}$, $R_{Le} \approx \frac{r_b}{\lambda_l(2\pi r_e W_e - n\pi r_b^2)}$, $R_{La} \approx \frac{1}{h_l \pi(r_e^2-r_i^2)}$

$$m_i C_{pi} \frac{\mathrm{dT}_i}{dt} = \frac{H_r}{2} + \frac{H_i}{2} - \frac{T_i - T_b}{\mathrm{R}_i + \mathrm{R}_1} - \frac{T_i - T_s}{\mathrm{R}_{sr}} \tag{20}$$

$$m_{Li} C_{pLi} \frac{\mathrm{dT}_{Li}}{dt} = \frac{H_i}{2} - \frac{T_{Li} - T_i}{\mathrm{R}_i} - \frac{T_{Li} - T_b}{\mathrm{R}_1} \tag{21}$$

$$m_b C_{pb} \frac{\mathrm{dT}_b}{dt} = \frac{H_i}{2} + \frac{H_e}{2} - \frac{T_b - T_{Li}}{\mathrm{R}_1} - \frac{T_b - T_{Le}}{\mathrm{R}_2} - \frac{T_b - T_\infty}{\mathrm{R}_{La}} \tag{22}$$

$$m_{Le} C_{pLe} \frac{\mathrm{dT}_{Le}}{dt} = \frac{H_e}{2} - \frac{T_{Le} - T_o}{\mathrm{R}_o} - \frac{T_{Le} - T_b}{\mathrm{R}_2} \tag{23}$$

$$m_o C_{po} \frac{\mathrm{dT}_o}{dt} = \frac{H_e}{2} - \frac{T_o - T_b}{\mathrm{R}_o + \mathrm{R}_2} - \frac{T_o - T_h}{\frac{R_{hrc} R_{hac}}{R_{hrc}+R_{hac}}} \tag{24}$$

$$m_h C_{ph} \frac{\mathrm{dT}_h}{dt} = -\frac{T_h - T_o}{\frac{R_{hrc} R_{hac}}{R_{hrc}+R_{hac}}} - \frac{T_h - T_\infty}{\frac{R_{hrv} R_{hav}}{R_{hrv}+R_{hav}}} \tag{25}$$

3.2 Thermal expansion and induced bearing load

Each component will expand with the rise of the temperature. Assuming that the distribution of the temperature in the touchdown bearing is linear.

The thermal expansion of the inner race, outer race, and ball is calculated as follows.

$$\varepsilon_i = \frac{\xi_i}{3}\frac{(1+\nu_i)r_s}{r_i+r_s}[\Delta T_i(2r_s + r_i) + \Delta T_{Li}(2r_i + r_s)] \tag{26}$$

$$\varepsilon_o = \frac{\xi_i}{3}\frac{(1+\nu_o)r_o}{r_o+r_j}[\Delta T_{Le}(2r_o + r_j) + \Delta T_j(2r_j + r_o)] \tag{27}$$

$$\varepsilon_b = \xi_b r_b \Delta T_b \tag{28}$$

where ε is the thermal expansion, ξ is the thermal expansion coefficient, ν is the poisson's ratio, ΔT is the temperature rise. The subscript i, e, b indicates the inner race, outer race and ball, respectively.

The interference change ε is as follows.

$$\varepsilon = \varepsilon_b + \frac{1}{2}(\varepsilon_i - \varepsilon_e)\cos\alpha_0 \tag{29}$$

where α_0 is the initial contact angle.

The thermally induced load is predicted by the following equation.

$$F_t = k \cdot \varepsilon^{1.5} \tag{30}$$

where k is the Hertzian contact stiffness.

The friction drag torque considering the induced load is calculated as follows.

$$M_1 = f_1(P_1 + F_t)d_m \tag{31}$$

4. Simulated results and discussion

Based on the previous illustrated dynamic and thermal model, simulation tests are demonstrated. By changing the initial speed and the friction coefficient, the results of the centroid motion locus, maximum contact forces and peak thermal power is obtained. Table 2 illustrates the parameters related to the rotor-bearing system. Two HRB 71908 angular contact ball bearing is mounted face to face. Table 3 shows the geometrical parameter of the bearing. Table 4 is the contact parameters of the rotor and the touchdown bearing.

Table 2 Specifications of rotor-touchdown bearings systems

Rotor		Inner race	
Mass of rotor, m_r	11.5 kg	Mass of inner race, m_b	0.048 kg
Diameter of rotor, d_r	39.7mm	Polar MOI of inner race, J_b	$2.33 \times 10^{-5}\ kg \cdot m^2$
Polar MOI of rotor, J_r	$5.806 \times 10^{-3}\ kg \cdot m^2$		

Table 3 Parameters of the type 71908 bearing (Unit:mm)

Bore diameter, d_1	40	Bearing width, B	12
Outer diameter, D_2	62	Ball diameter, d	5.5

Table 4 Parameters of the contact

Stiffness coefficient of contact, k_1	$1.988 \times 10^9\ N \cdot m^{-10/9}$
Damping coefficient of contact, c_1	$1000N \cdot$s/m
Stiffness coefficient of contact, k_2	$2.47 \times 10^5\ N \cdot mm^{-1.5}$
Damping coefficient of contact, c_2	$750N \cdot$s/m
Radial clearance between rotor and bearing, s	0.15 mm

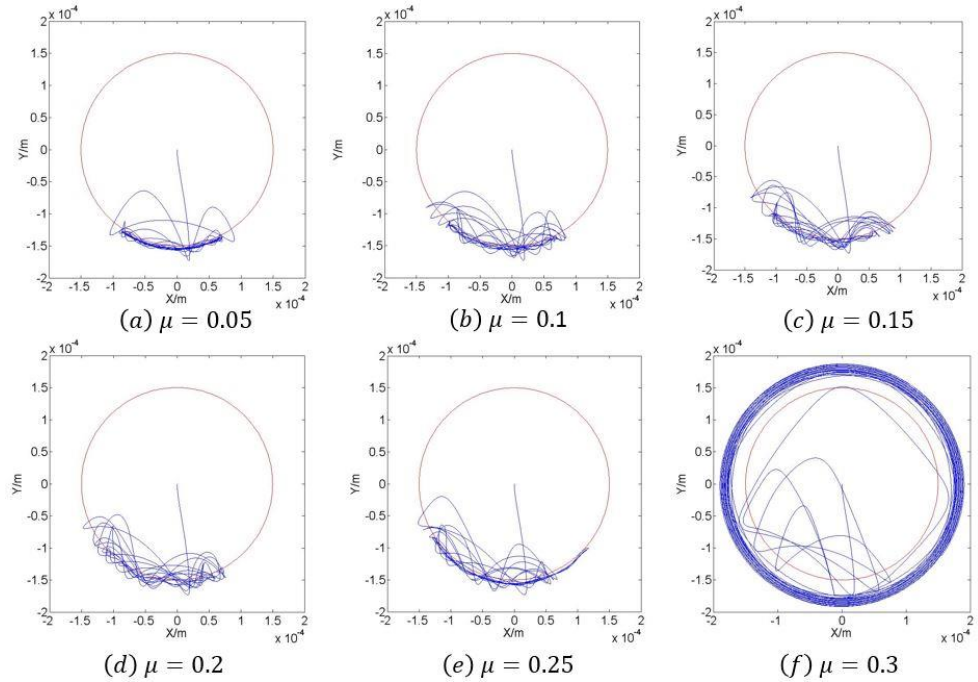

Fig. 3 The simulated orbits of the rotor when dropping at the rotating speed of 8000r/min and the friction coefficients of (a)0.05; (b)0.1; (c)0.15; (d)0.2; (e)0.25; (f)0.3, respectively.

The simulated results of the centroid motion locus of the rotor when dropping at the speed of 8000r/min and the friction coefficient from 0.05 to 0.3 is illustrated in Fig.3. Pendulum vibration can be observed when the friction coefficient is not higher than 0.25. The backward whirl is not observed until the sliding friction coefficient has reached 0.3.

4.1 Backward whirl critical rotation speed

As can be shown in Fig.3, the probability of triggering the backward whirl motion increases with the increase of the sliding friction coefficient. The reliability, however, decreases considerably. For the specific rotor-bearing system, a critical speed at each friction coefficient between the rotor and the inner race exists. The critical speed can be defined as 'Backward whirl critical rotating speed', which has been shown in Fig.4. The pendulum vibration will occur when the point of working condition is below the curve, while backward whirl will occur when the point of working condition is above the curve.

It can be observed in Fig. 4 that the safe landing of the rotor is strongly influenced by the initial rotating speed and the friction coefficient between the rotor and the inner race.

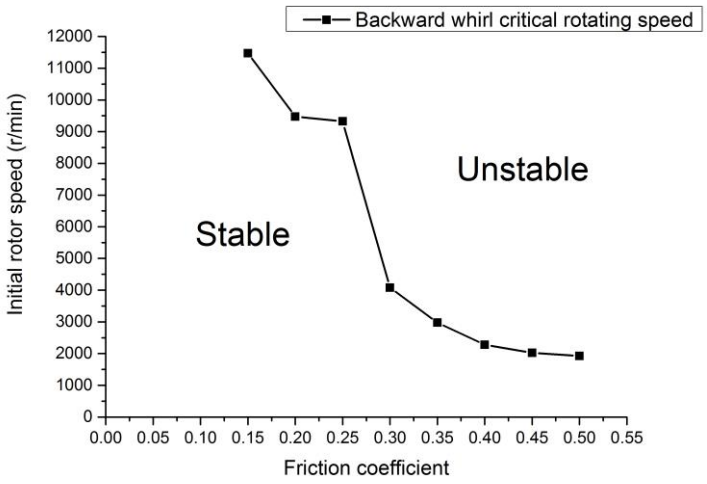

Fig. 4 Backward whirl critical rotating speed.

4.2 Influence of the rotating speed and friction coefficient on the contact force

Figure 5 demonstrates the influence of the rotating speeds and friction coefficients on the maximum contact forces. The force of first contact after the free fall motion is about 900N. The points in Fig. 5 above 900N indicates that the maximum contact force takes place at a certain contact after the first contact. The maximum contact forces keep almost constant when both the rotating speeds and the friction coefficients are comparatively low. It increases with the growth of the rotating speed and the friction coefficient with high rotating speeds, high friction coefficients or both. The maximum contact forces of the backward whirl is not included in Fig. 5, as the precise results of the backward whirl is strongly influenced by the precision of the stiffness and damping of the housing as well as the flexibility of the rotor. The calculation of the maximum contact force contributes to the analysis of the damage of the contact surface of the rotor and the inner race.

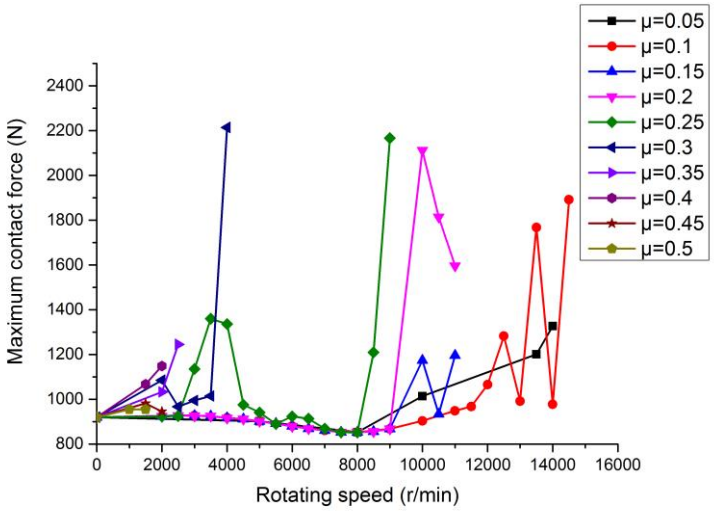

Fig. 5 The relationship between the maximum contact force and rotating speed and the friction coefficient.

4.3 Influence of the rotating speed and friction coefficient on the peak thermal power

Figure 6 illustrates the peak thermal power of different rotating speeds and the friction coefficients. It can be observed that the peak thermal power increases with the incline of the friction coefficients and the rotating speeds. The reliability of the touchdown bearings is getting worse with the increase of peak thermal power.

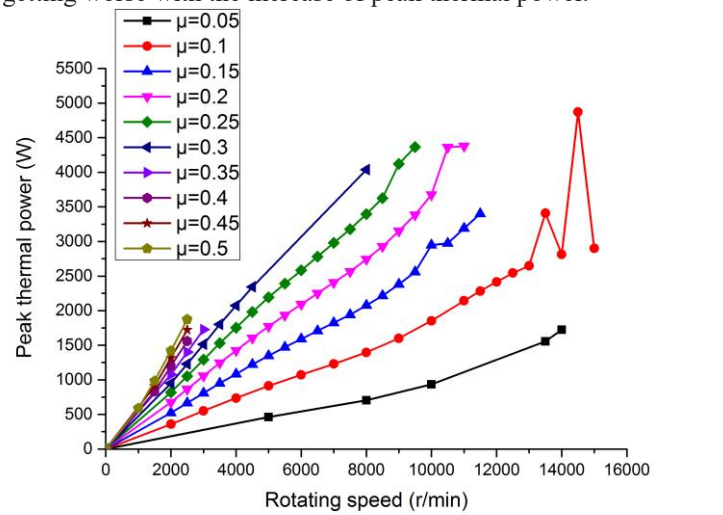

Fig. 6 The relationship between the peak thermal power and the rotating speed and friction coefficient.

5. Conclusion

The dynamic and thermal model during touchdown events has been established in the paper. Simulations under different working conditions have been conducted for the specific AMB system. The results of the centroid motion locus

of the rotor, maximum contact forces and the peak thermal power between the rotor and the inner race has been analyzed.

The simulation results show that the backward whirl critical speed exists for the certain AMB system. The points of the initial working conditions below the critical speed indicates that the orbit response is the pendulum vibration, while the points above the critical speed means that the orbit response is the backward whirl which will pose a threat to the AMB system. For the safety consideration, the initial working conditions below the critical speed is more desirable.

The maximum contact forces keep almost constant when both the rotating speeds and the friction coefficients are low. It increases with the growth of the rotating speed and the friction coefficient with high rotating speeds, high friction coefficients or both. The peak thermal power increases with the incline of the friction coefficient and the rotating speed.

6. References

Fumagalli, M., Modelling and Measurement Analysis of the Contact Interaction between a High Speed, ETH Zurich (1997).

Sheng Zeng, Motion of AMB rotor in backup bearings. Journal of Vibration and Acoustics, Vol. 124 (2002), pp.460-464

ShengZeng, Modelling and experimental study of the transient response of an active magnetic bearing rotor during rotor drop on back-up bearings. Proceedings of the Institution of Mechanical Engineers Part I Journal of Systems & Control Engineering. (2003), pp505-517.

Kärkkäinen Antti, Helfert Marlene, Aeschlimann Beat, Mikkola Aki. Dynamic Analysis of Rotor System With Misaligned Retainer Bearings, Journal of Tribology, Vol 130, No.2 (2008), pp:319-320.

Kärkkäinen Antti, Dynamic simulations of rotors during drop on retainer bearings, Lappeenranta University of Technology (2007)

Guangyoung Sun, A high fidelity ball bearing and damper model including thermal effects for magnetic suspension auxiliary service and blade loss simulation, Texas A&M University (2003)

Jung Gu Lee, Alan Palazzolo, Catcher bearing life prediction using a rainflow counting approach, Journal of Tribology, Vol. 134, No.3 (2012)

Yulan Zhao, Guojun Yang, Zhengang Shi, Lei Zhao, Thermal analysis and simulation of touchdown bearings and its application in the high temperature reactor-10, Journal of Tribology, Vol.138, No.1 (2016)

Tedric A. Harris, Michael N. Kotzalas. Rolling bearing analysis (5th edition): Essential concepts of bearing technology (2007), p.50, Taylor & Francis.